

# Excess Colloid Retention in Porous Media as a Function of Colloid Size, Fluid Velocity, and Grain Angularity

MEIPING TONG AND  
WILLIAM P. JOHNSON\*

Department of Geology and Geophysics, The University of Utah, Salt Lake City, Utah 84112

The deposition and re-entrainment behaviors of five sizes of carboxylate-modified microspheres (ranging from 0.1 to 2.0  $\mu\text{m}$ ) were examined both in porous media and impinging jet systems under a variety of environmentally relevant pore fluid velocities (2–8  $\text{m day}^{-1}$ ), and in both the absence and the presence of an energy barrier to deposition. The magnitudes of the deposition efficiencies were compared among the porous media and impinging jet systems under equivalent fluid velocities, solution chemistries, and surface chemistries. The observed deposition efficiencies were factors of about 5 to 50 greater in the porous media relative to the impinging jet across the entire size range of microspheres examined, demonstrating that this excess deposition in porous media is relevant to a wide range of colloid sizes. The magnitude of excess deposition increased with increasing fluid velocity, and was greatest for the smallest colloids (0.1  $\mu\text{m}$ ). A range between 15% and 40% of the excess retained colloids were released upon introduction of low ionic strength solution, indicating that they were retained via secondary energy minima without direct contact with the grain surfaces. The observations indicate that pore geometry is a critical governor of colloid deposition in the presence of an energy barrier, even in porous media composed of spherical collectors. A portion of this excess deposition results from retention in flow stagnation zones.

## Introduction

Surfaces of environmental colloids (biological and nonbiological) and porous media typically display bulk negative charge, yielding overall repulsive electric double layer energies between them. Despite the presence of this energy barrier, colloid deposition onto overall like-charged grain surfaces is well demonstrated. A number of mechanisms have been proposed to explain colloid deposition in porous media in the presence of an energy barrier, such as localized nanoscale patches of attractive surface charge (1–4), grain surface roughness (5, 6), straining (7–11), and deposition in the weakly attractive energy minimum (secondary energy minimum) outboard (at greater separation distances) from the interaction energy barrier (12–17).

Colloid deposition flux in the presence of an energy barrier is normalized to that in the absence of an energy barrier to yield the deposition efficiency ( $\alpha$ ). Recent experiments demonstrate that  $\alpha$  is greater in porous media relative to flat surfaces (e.g., impinging jet systems) under equivalent

conditions. Values of  $\alpha$  observed for a bacterial strain (1.7  $\mu\text{m}$  effective diameter) in quartz sand were factors of 10–100 greater than those observed on quartz substrata in an impinging jet system under equivalent conditions (15, 16). Likewise, values of  $\alpha$  observed for carboxylate-modified polystyrene latex microspheres (1.1 and 5.7  $\mu\text{m}$  diameter) were factors of 2–3 greater than those observed on quartz substrata in an impinging jet under equivalent conditions (17).

In the above studies, the observed excess deposition efficiency in the porous media was attributed to colloid association with the grain surface via secondary energy minima and retention in rear flow stagnation zones (15–17). The rationale for retention involving secondary energy minima was the observed release of the majority of deposited colloids upon introduction of low ionic strength solution, indicating association with grain surfaces via attractive colloidal forces that were eliminated in response to decreased ionic strength, i.e., the secondary energy minimum. Since secondary energy minimum-associated colloids would be subject to fluid drag and transport along the grain surface, their retention requires the presence of flow stagnation zones, e.g., rear flow stagnation zones. In contrast, retention in an impinging jet system (flat, smooth surface) requires association with the surface via the primary energy minimum, since the absence of flow stagnation zones would allow secondary energy minimum-associated colloids to be swept from system (15–18).

Since fluid drag increases with increasing colloid size, one might expect the discrepancy between porous media and impinging jet deposition efficiencies to increase with increasing colloid size. The previous few investigations regarding excess  $\alpha$  concerned colloid sizes in the range of 1.0  $\mu\text{m}$  diameter and larger (15–17). The relevance of excess  $\alpha$  to colloids smaller than 1.0  $\mu\text{m}$  in diameter is uncertain, since colloid size may dictate not only the fluid drag force, but also may govern the number of colloids retained in flow stagnation zones. Hence, the relationship between colloid size and excess  $\alpha$  is not clear, and requires investigation. Furthermore, since fluid drag increases with increasing fluid velocity, excess  $\alpha$  would be expected to increase with increasing fluid velocity. However, the capacities of flow stagnation zones are an uncertain function of fluid velocity. Hence, the relationship between fluid velocity and excess deposition efficiency also requires examination.

Previous studies of excess deposition primarily concerned porous media composed of angular collectors (quartz sand). Recent experiments suggest that colloid deposition in the presence of an energy barrier occurs dominantly in association with grain-to-grain contacts (19, 20), which are more prevalent in angular relative to spherical porous media (19, 20). Hence, another issue requiring investigation is the significance of excess  $\alpha$  in porous media composed of spherical grains.

The objective of this paper is to demonstrate that the magnitude of excess  $\alpha$  in porous media composed of spherical collectors (grains) is large (ranging from 5 to 50) across the colloid size range examined here (0.1–2.0  $\mu\text{m}$  diameter), demonstrating that this excess deposition is relevant to a wide range of colloid sizes, as well as to angular and spherical porous media. We discuss the trends in excess  $\alpha$  versus colloid size and fluid velocity. These observations demonstrate that the geometry of the pore domain is paramount to colloid deposition in the presence of an energy barrier for a wide spectrum of colloid sizes and for both spherical and angular porous media collectors.

\* Corresponding author phone: (801) 581-5033; fax: (801) 581-7065; e-mail: wjohnson@mines.utah.edu.

## Materials and Methods

**Microspheres.** Spherical fluorescent carboxylate-modified polystyrene latex microspheres (Molecular Probes, Inc., Eugene, OR) of five sizes (diameters of 0.1, 0.2, 0.5, 1.0, and 2.0  $\mu\text{m}$ , with negative surface charge densities of 0.3207, 0.282, 0.1419, 0.0175, and 0.1076 meq  $\text{g}^{-1}$ , respectively) were used in all experiments except as noted. The 0.1, 0.2, 0.5, 1.0, and 2.0  $\mu\text{m}$  microsphere stock suspensions had particle concentrations of  $3.6 \times 10^{13}$ ,  $4.5 \times 10^{12}$ ,  $2.9 \times 10^{11}$ ,  $2.7 \times 10^{10}$ , and  $4.5 \times 10^9$  microspheres  $\text{mL}^{-1}$ , respectively. The stock solutions contained  $\text{NaN}_3$  (2 mM); whereas the 2.0  $\mu\text{m}$  microsphere stock suspension also included 0.01% Tween-20.

Prior to injection, stock solutions for the 0.1, 0.2, 0.5, and 1.0  $\mu\text{m}$  microspheres were diluted in NaCl solution to achieve a nominal influent concentration ( $C_0$ ) of  $1.0 \times 10^7$  particles  $\text{mL}^{-1}$  at the desired ionic strength (NaCl), plus MOPS buffer (2.2 mM), yielding a solution pH of 6.72. The stock solution for the 2.0  $\mu\text{m}$  microspheres was first diluted 10 times in pure (Milli-Q) water (Millipore Corp. Bedford, MA), and was washed three times to remove Tween-20. Washing involved centrifugation (10 000g for 10 min at 4  $^\circ\text{C}$ ), followed by decanting, and addition of pure water. Following washing, the 2.0  $\mu\text{m}$  microsphere solution was diluted in NaCl solution to achieve a nominal influent concentration ( $C_0$ ) of  $1.0 \times 10^6$  at the desired ionic strength (NaCl) plus MOPS buffer (2.2 mM), yielding a solution pH of 6.72.

Deposition in the packed porous media column and the impinging jet systems was examined both in the absence and presence of an energy barrier. Experiments in the presence of an energy barrier to deposition were conducted at an ionic strength of 0.02 M for 0.1, 0.2, 0.5, and 1.0  $\mu\text{m}$  microsphere sizes, and at an ionic strength of 0.05 M for 2.0  $\mu\text{m}$  microspheres. The corresponding  $\zeta$ -potentials for the 0.1, 0.2, 0.5, 1.0, and 2.0  $\mu\text{m}$  microspheres were about -23, -27, -41, -59, and -43 mV, respectively. Measurements to determine  $\zeta$ -potentials are described in detail in the Supporting Information.

Experiments performed in the absence of an energy barrier were conducted at various ionic strengths depending on the strategy used to eliminate the energy barrier. For the 1.0  $\mu\text{m}$  microspheres, conditions absent an energy barrier were generated by use of amine-functionalized polystyrene latex microspheres (Molecular Probes, Inc., Eugene, OR) at an ionic strength of 0.001 M. The amine-functionalized microspheres had a stock concentration of  $4.5 \times 10^{10}$  microspheres  $\text{mL}^{-1}$ , a diameter of 0.93  $\mu\text{m}$ , and a positive surface charge of 0.9176 meq  $\text{g}^{-1}$ . Since amine-modified microspheres were not commercially available in the 0.1, 0.2, 0.5, and 2.0  $\mu\text{m}$  sizes, elimination of the energy barrier for the 0.1, 0.2, 0.5, and 2.0  $\mu\text{m}$  microspheres was achieved by lowering solution pH to 2 (HCl addition) and increasing the solution ionic strength to 0.05 M (NaCl). The corresponding  $\zeta$ -potentials for the 0.1, 0.2, 0.5, 0.93, and 2.0  $\mu\text{m}$  microspheres were about -13.8, -2.3, -5.2, +9.2, and -5.4 mV, respectively (Supporting Information).

**Porous Media Experiments.** *Porous Media.* Spherical soda lime glass beads (Cataphote Inc. Jackson, MS) and quartz sand (Unimin Corp., New Canaan, CT) with sizes ranging from 417 to 600  $\mu\text{m}$  were used for microsphere deposition experiments in porous media. The procedure used for cleaning the glass beads and quartz sand is provided in previous publications (21–23), as well as in the Supporting Information. The  $\zeta$ -potentials of the glass beads were -51 and -56 mV at ionic strengths of 0.02 and 0.05 M, respectively (pH 6.72); whereas the  $\zeta$ -potential of the glass beads at pH 2 and an ionic strength of 0.05 M was -10 mV (Supporting Information).

*Porous Media Experimental Conditions.* Cylindrical Plexiglass columns (20 cm long, 3.81 cm i.d.) were dry-packed

with glass beads or quartz sand, flushed with  $\text{CO}_2$ , and equilibrated with microsphere-free solution. The procedure of packing and pre-equilibration is described in previous publications (21–24), and in the Supporting Information.

After pre-equilibration, a solution with microspheres was injected (3 pore volumes). This was followed by elution with microsphere-free solution (7 pore volumes). Selected experiments included a subsequent phase to examine the release of retained microspheres in response to further elution with the following solutions: (1) microsphere-free solution at the pH and ionic strength of the injection and elution solutions (2 pore volumes); (2) low ionic strength solution (0.0002 M) (without microspheres) (2 pore volumes); pH 11 solution (adjusted by NaOH) (without microspheres) (3 pore volumes). The low ionic strength solution was introduced to eliminate the secondary energy minimum, whereas the pH 11 solution was introduced to reverse any positively charged domains (e.g., metal oxide impurities) on the grain surfaces.

During injection, the microsphere suspension reservoirs were sonicated for 1 min per hour to minimize aggregation, as verified by flow cytometric analyses (Supporting Information). The flow rate was varied between experiments to produce pore water velocities at 2, 4, and 8  $\text{m day}^{-1}$ . Experiments performed in the absence of an energy barrier involved all three fluid velocities, whereas experiments performed in the presence of an energy barrier involved only the higher two fluid velocities (4 and 8  $\text{m day}^{-1}$ ) due to the occurrence of ripening at the lower fluid velocity. The suspensions and solutions were injected in up-flow mode using a syringe pump (Harvard Apparatus, Inc, Holliston, MA).

*Sample Collection and Analysis.* Column effluent samples were collected in 5 mL polystyrene tubes using a fraction collector (CF-1, Spectrum Chromatography, Houston, TX). Following the experiment, the porous media was dissected into ten 2-cm-long segments, as the porous media was released from the column under gravity. Retained colloids were recovered by placing porous media segments (2 cm) into specified volumes of Milli-Q water and sonicating for 1 min, followed by manual vigorous shaking for 0.5 min. Aqueous effluent samples, and supernatant samples from recovery of retained microspheres, were analyzed using flow cytometry (BD FACScan, Becton Dickinson & Co., Franklin Lakes, NJ); details are provided in Li et al. (21). The area under the breakthrough-elution curve was integrated to yield the number of microspheres that exited the column. The colloids recovered from all segments of the sediment were summed to determine the total number of retained colloids. The overall recovery (mass balance) of colloids was determined by summing the numbers of retained colloids and colloids that exited the column. The overall recovered number of colloids was divided by the number of injected colloids to express the mass balance as a percentage.

The transport and deposition of microspheres in porous media was modeled using an advection-dispersion equation that includes removal from, and re-entrainment to, the aqueous phase:

$$\frac{\partial C}{\partial t} = -v \frac{\partial C}{\partial x} + D \frac{\partial^2 C}{\partial x^2} - k_f C + \frac{\rho_b}{\theta} k_r S_r \quad (1)$$

where  $C$  is the concentration of microspheres in the aqueous phase (spheres per unit volume of fluid),  $t$  is the travel time,  $x$  is the travel distance,  $v$  is the fluid velocity,  $D$  is the dispersion coefficient of the colloid particles,  $\theta$  is the porosity,  $\rho_b$  is the bulk density of sediment, and  $k_f$  and  $k_r$  are rate coefficients for microsphere deposition to and re-entrainment from the solid phase, respectively.  $S_r$  is the reversibly retained microspheres concentration on the solid phase (spheres per unit mass of sediment) and can be further

expressed as

$$S_r = S f_r \quad (2)$$

where  $S$  is the total deposited sphere concentration and  $f_r$  is the fraction of reversibly retained spheres. The total deposited microsphere concentration ( $S$ ) is related to  $C$  as follows:

$$\frac{\rho_b}{\theta} \frac{\partial S}{\partial t} = k_f C - \frac{\rho_b}{\theta} k_r S_r \quad (3)$$

A one-dimensional discrete random-walk particle-tracking model was used to solve eqs 1 and 2 under the conditions of the porous media experiments, and details of implementation of the governing equation can be found in other publications (21, 25, 26). It is important to note that the probabilistic approach used in the particle tracking model decouples the parameters  $k_f$  and  $f_r$ , whereas this decoupling is not apparent in the equations as written in continuum form (eqs 1 and 2).

The deposition rate coefficient in porous media ( $k_f$ ) was also calculated from the collector efficiency ( $\eta$ ) as follows:

$$k_f = \frac{3}{2} \frac{(1 - \theta)}{d_c} \alpha \eta v \quad (4)$$

where  $\theta$  is the sediment porosity,  $d_c$  is the collector (sediment grain) diameter,  $v$  is the fluid velocity, and  $\alpha$  is the collision efficiency, which is the number of colloid attachments per

number of collisions. Different correlation equations are available to estimate  $\eta$ , e.g., the correlation equations developed by Rajagopalan and Tien (27, 28) and Tufenkji and Elimelech (29), which are abbreviated below as the R-T and T-E equations, respectively.

**Impinging Jet Experiments.** *Substrata Preparation.* Glass microscope slides (Fisher Scientific, Inc.) of dimension  $25 \times 75 \times 1$  mm were used in the impinging jet flow cell. The SC-1 cleaning procedure (30) was used for cleaning the glass substrata, as described in a previous publication (18) and in the Supporting Information. The  $\zeta$ -potentials of glass substrata were similar to those of glass beads under equivalent experimental conditions ( $-51$  and  $-56$  mV at ionic strengths of 0.02 and 0.05 M at pH of 6.72, respectively; and  $-10$  mV at pH 2 and an ionic strength of 0.05 M) (Supporting Information).

*Impinging Jet Experimental Conditions.* Colloid deposition experiments were performed in an impinging jet system (radial stagnation point flow) for the range of microsphere sizes, fluid velocities, and solution chemistry conditions utilized in porous media experiments. To increase the accuracy of flux determination, the experiments were continued until a minimum of 60 microspheres was deposited in the observation area. The duration of the experiments ranged from 10 to 60 min in the absence of an energy barrier to deposition, whereas the duration of experiments ranged from 3 to 9 h in the presence of an energy barrier to deposition. The corresponding numbers of deposited colloids ranged from 60 to 400. An example net deposition curve is given in the Supporting Information.

**TABLE 1. Porous Media Experimental Conditions, Mass Balances, Observed Transport Parameters (via the Particle-Tracking Model), and Simulated Deposition Rate Coefficient ( $k_f$ ) (Using the R-T Correlation Equation)<sup>a</sup>**

diameter ( $\mu\text{m}$ )	ionic strength (M)	pH	average pore water velocity ( $\text{m day}^{-1}$ )	mass recovery <sup>b</sup> %	retained <sup>c</sup> %	$k_f$ ( $\text{h}^{-1}$ )	$k_r$ ( $\text{h}^{-1}$ )	$f_r$	RT $k_f$ ( $\text{h}^{-1}$ )	$\alpha$	
0.1	0.02	6.72	4	86.0	35.2	0.72	0.10	0.07		0.072	
			8	101.1	2.2	0.06	0.45	0.40		0.003	
	0.05	2	4	101.3	101.1	10.0	0	0	26.1		
			8	91.8	91.8	20.0	0	0	32.9		
	0.2	0.02	6.72	4	93.1	22.2	0.26	0.15	0.3		0.0325
				8	105.2	14.6	0.25	0.5	0.03		0.0172
0.05		2	4	105.3	105.3	8.0	0	0	16.5		
			8	88.3	88.3	14.5	0	0	20.7		
0.5		0.02	6.72	4	99.9	3.6	0.063	0.2	0.4		0.0097
				4 <sup>d</sup>	105.2	34.6	0.45	0.28	0.35		0.045
	8		100.0	2.2	0.06	0.48	0.38		0.0086		
			2	100.02	100.01	3.7	0	0	7.21		
	4		81.5	81.5	6.5	0.1	0	9.04			
			8	98.9	97.3	7.0	0	0	11.4		
	2 <sup>d</sup>		100.03	100.03	6.0	0	0				
			4 <sup>d</sup>	80.4	80.4	10.0	0	0			
	8 <sup>d</sup>		100.0	100.0	14.0	0	0				
1.0	0.02	6.72	4	87.7	17.0	0.25	0.3	0.42		0.0625	
			8	100.1	7.9	0.17	0.5	0.21		0.034	
0.93	0.001	6.72	2	101.1	99.6	1.9	0.03	0.05	4.93		
			4	101.8	100.7	4.0	0.1	0.01	6.03		
			8	97.6	92.9	5.0	0.1	0.01	7.55		
2.0	0.05	6.72	4	93.3	59.2	0.92	0.1	0.02		0.2244	
			8	92.7	26.3	0.56	0.11	0.1		0.0862	
	0.05	2	2	91.7	91.5	2.5	0	0	4.65		
			4	102.4	101.2	4.1	0	0	5.27		
	8		88.0	85.9	6.5	0.05	0.01	6.21			

<sup>a</sup> Conditions absent an energy barrier correspond to ionic strength 0.05 M and pH 2 for the 0.1, 0.2, 0.5, and 2.0  $\mu\text{m}$  microspheres. For the 1.0  $\mu\text{m}$  microspheres, amine-functionalized microspheres (0.93  $\mu\text{m}$ ) were used to represent conditions absent an energy barrier. Deposition efficiency ( $\alpha$ ) does not apply to conditions absent an energy barrier. <sup>b</sup> Mass recovery % refers to percent recovery of injected microspheres via effluent and via desorption following dissection. <sup>c</sup> Retained % refers to percent recovery of injected microspheres via desorption following dissection. <sup>d</sup> Experiments were conducted in quartz sand. All other porous media experiments were conducted in glass beads.

**TABLE 2. Impinging Jet Experimental Conditions, Observed Deposition Fluxes, and Simulated Deposition Fluxes<sup>a</sup>**

diam. ( $\mu\text{m}$ )	ionic strength (M)	pH	jet velocity ( $\text{m s}^{-1}$ )	experimental deposition flux ( $\text{m s}^{-1}$ )	simulated deposition flux ( $\text{m s}^{-1}$ )	$\alpha$
0.1	0.02	6.72	$1.70 \times 10^{-3}$	$1.81 \times 10^{-9}$	0	0.00162
			$2.97 \times 10^{-3}$	0	0	0
			$1.70 \times 10^{-3}$	$1.12 \times 10^{-6}$	$4.50 \times 10^{-7}$	
0.2	0.02	6.72	$1.70 \times 10^{-3}$	$2.14 \times 10^{-9}$	0	0.00372
			$2.97 \times 10^{-3}$	0	0	0
			$1.06 \times 10^{-3}$	$4.08 \times 10^{-7}$	$1.20 \times 10^{-7}$	
0.5	0.02	6.72	$1.70 \times 10^{-3}$	$7.65 \times 10^{-10}$	0	0.00227
			$2.97 \times 10^{-3}$	0	0	0
			$1.06 \times 10^{-3}$	$1.86 \times 10^{-7}$	$9.83 \times 10^{-8}$	
1.0	0.02	6.72	$1.70 \times 10^{-3}$	$3.08 \times 10^{-9}$	0	0.0138
			$2.97 \times 10^{-3}$	0	0	0
			$1.70 \times 10^{-3}$	$4.96 \times 10^{-7}$	$1.63 \times 10^{-7}$	
0.93	0.001	6.72	$1.70 \times 10^{-3}$	$1.41 \times 10^{-7}$	$8.59 \times 10^{-8}$	
			$1.70 \times 10^{-3}$	$2.23 \times 10^{-7}$	$9.38 \times 10^{-8}$	
			$2.97 \times 10^{-3}$	$2.68 \times 10^{-7}$	$9.60 \times 10^{-8}$	
2.0	0.05	6.72	$1.70 \times 10^{-3}$	$3.15 \times 10^{-9}$	0	0.0137
			$2.97 \times 10^{-3}$	0	0	0
			$1.06 \times 10^{-3}$	$1.63 \times 10^{-7}$	$7.85 \times 10^{-8}$	
2.0	0.05	2	$1.70 \times 10^{-3}$	$2.29 \times 10^{-7}$	$1.08 \times 10^{-7}$	
			$2.97 \times 10^{-3}$	$2.69 \times 10^{-7}$	$1.32 \times 10^{-7}$	

<sup>a</sup> All impinging jet experiments were conducted on glass substrata. Conditions absent an energy barrier correspond to ionic strength 0.05 M and pH 2 for the 0.1, 0.2, 0.5, and 2.0  $\mu\text{m}$  microspheres. For the 1.0  $\mu\text{m}$  microspheres, amine-functionalized microspheres (0.93  $\mu\text{m}$ ) were used to represent conditions absent an energy barrier. Deposition efficiency ( $\alpha$ ) does not apply to conditions absent an energy barrier.

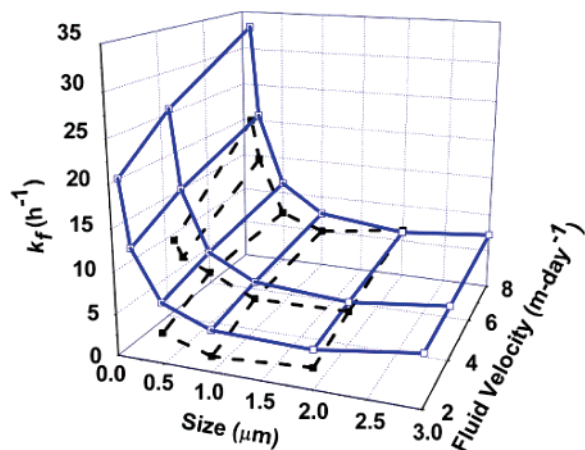


**FIGURE 1. Simulated (open symbols) and observed (closed symbols) deposition rate coefficients ( $k_f$ ) in the absence of an energy barrier to deposition for all five microspheres sizes as a function of fluid velocity in glass beads. Simulated deposition rate coefficients were calculated using the R–T correlation equation. Observed deposition rate coefficients (connected by dashed lines) were slightly lower than corresponding simulated deposition rate coefficients.**

Porous media and impinging jet experiments were performed under comparable near-surface fluid velocities. Since the porous media and impinging jet systems yield different fluid velocity distributions, the fluid velocities in the two systems were chosen to favor (slightly) colloid deposition in the impinging jet, as described in the Supporting Information. The fluid velocities used in the impinging jet were  $1.06 \times 10^{-3}$ ,  $1.70 \times 10^{-3}$ , and  $2.97 \times 10^{-3} \text{ m s}^{-1}$ . Detailed fluid velocity histograms of the impinging jet and porous media systems are provided in the Supporting Information.

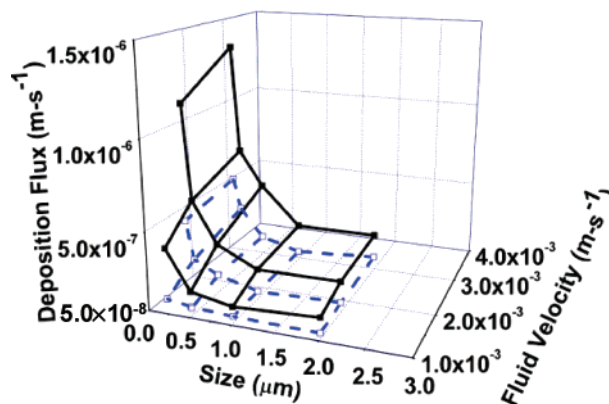


**FIGURE 2. Simulated (open symbols) and observed (closed symbols) deposition fluxes in the absence of an energy barrier to deposition for all five microsphere sizes as a function of fluid velocity in the impinging jet system. Simulated deposition fluxes were calculated using the P2DJET model. Simulated deposition fluxes (connected by dashed lines) were slightly lower than corresponding observed deposition fluxes.**

*Sample Collection and Analyses.* Details on the impinging jet system and the corresponding image analysis are provided in a previous publication (18) and in the Supporting Information. The deposition flux was determined from the slope of the initial (linear) portion of the curve representing the number of deposited microspheres versus time. This slope was divided by the observation area ( $450 \mu\text{m} \times 336 \mu\text{m}$ ) and the influent microsphere concentration to obtain a normalized deposition flux ( $\text{m s}^{-1}$ ).

The transport and deposition of microspheres in the impinging jet was simulated using a numerical model (P2DJET) (18). The numerical simulations accounted for the various forces acting on the colloid: Brownian diffusion, fluid drag, gravity, virtual mass, van der Waals, and electric double layer forces. The details of the model are given in a previous publication (18) and the parameters used in the simulations exactly reflected experimental conditions.

For both porous media and impinging jet experiments, the deposition flux in the presence of an energy barrier is presented in terms of the deposition efficiency ( $\alpha$ ), which is the ratio of the deposition flux in the presence relative to the absence of an energy barrier. The deposition flux is quantified in the porous media using the deposition rate coefficient ( $\text{h}^{-1}$ ), and in the impinging jet using the normalized deposition flux ( $\text{m s}^{-1}$ ). The experimental conditions for porous media and impinging jet experiments are summarized in Tables 1 and 2.

## Results and Discussion

**Deposition Flux in the Absence of an Energy Barrier to Deposition.** In the absence of an energy barrier, observed and simulated deposition rate coefficients (porous media) and deposition fluxes (impinging jet) increased with increasing fluid velocity for all microsphere sizes (Tables 1 and 2 and Figures 1 and 2). Observation and simulation agreed closely, with the largest discrepancy being about a factor of 2 for the 0.1  $\mu\text{m}$  diameter microspheres.

For all fluid velocities examined, the observed minimum deposition rate coefficient (porous media) and deposition flux (impinging jet) corresponded to the 1.0  $\mu\text{m}$  diameter colloids. The simulated minimum corresponded to the 2.0  $\mu\text{m}$  diameter colloids in the porous media, whereas the simulated minimum corresponded to the 1.0  $\mu\text{m}$  diameter colloids in the impinging jet. However, this discrepancy is minor since the observed and simulated values were similar for the 1.0 and 2.0  $\mu\text{m}$  diameter colloids in both systems. These results show that in the absence of an energy barrier,

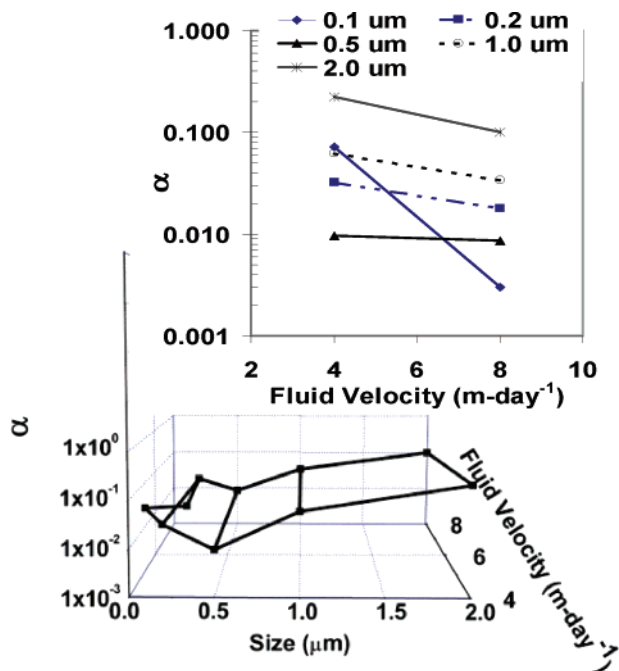


FIGURE 3. Observed deposition efficiencies for all sizes of microspheres on glass beads as a function of fluid velocity in the presence of an energy barrier to deposition at an ionic strength = 0.02 M and pH = 6.72 (ionic strength = 0.05 M for the 2.0  $\mu\text{m}$  microspheres). The inset highlights the trend of deposition efficiency as a function of fluid velocity for all five microsphere sizes.

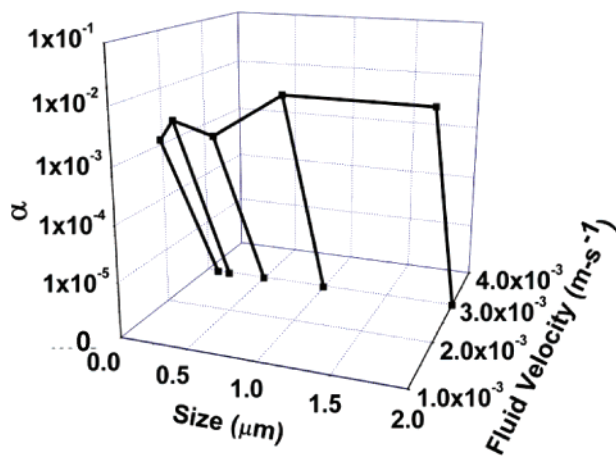


FIGURE 4. Observed deposition efficiencies for all sizes of microspheres on the glass substratum as a function of fluid velocity in the presence of an energy barrier to deposition at an ionic strength = 0.02 M and pH = 6.72 (ionic strength = 0.05 M for the 2.0  $\mu\text{m}$  microspheres).

deposition fluxes increase with increasing fluid velocity as predicted by theory, and minimum deposition fluxes correspond to colloid sizes in the range between 1.0 and 2.0  $\mu\text{m}$ .

**Deposition Efficiency in the Presence of an Energy Barrier to Deposition.** In the presence of an energy barrier, deposition efficiencies ( $\alpha$ ) (deposition flux in the presence relative to the absence of an energy barrier) decreased with increasing fluid velocity as shown in Figures 3 and 4. This was observed for all five microsphere sizes for both the porous media (Figure 3) and the impinging jet (Figure 4) systems. Values of  $\alpha$  did not show a minimum corresponding to the 1.0–2.0  $\mu\text{m}$  diameter size range (observed in the absence of an energy barrier), possibly due to the differences in retention mechanisms operating in the presence versus the absence of an energy barrier, and possibly due to differences in surface chemistries for the different microsphere sizes (different

batches), which controls the height of the energy barrier to deposition.

If  $\alpha$  were constant with changes in fluid velocity, it would be reasonable to conclude that fluid drag influences colloid deposition equivalently in the presence versus the absence of an energy barrier. The fact that  $\alpha$  decreases with increasing fluid velocity indicates that colloid deposition in the presence of an energy barrier is relatively susceptible to mitigation by fluid drag, as previously described in several publications (17, 18, 31, 32).

**Comparison of Deposition Efficiency in Porous Media vs Impinging Jet.** Despite the obvious differences in pore domain geometry between the porous media and impinging jet systems, deposition fluxes (absence of energy barrier) and  $\alpha$  (presence of energy barrier) trended similarly, that is,  $k_f$  increased with increasing fluid velocities in both systems, and  $\alpha$  decreased with increasing fluid velocity in both systems. However, an important difference between the two systems is the magnitudes of the observed values of  $\alpha$ .

The observed values of  $\alpha$  were greater (by factors of about 5–50) in the porous media relative to the impinging jet across the entire size range of microspheres examined (Tables 1 and 2, and Figure 5). This observed “excess”  $\alpha$  is in agreement with several previous studies in angular porous media (quartz sand) (15–17). However, these previous studies concerned colloids in the size range of about 1.0  $\mu\text{m}$  (diameter) and larger. In this study we have extended demonstration of the excess deposition efficiency to colloid sizes an order of magnitude lower (0.1  $\mu\text{m}$  diameter). The significant excess deposition observed for the 0.1  $\mu\text{m}$  colloids can also be expected to hold for somewhat smaller sizes; however, colloids smaller than 0.1  $\mu\text{m}$  are difficult to examine directly using optical microscopy. At some size less than 0.1  $\mu\text{m}$ , one would expect the fluid drag forces to decrease to the point that no excess deposition efficiency would be observed. The colloidal size range from 0.1  $\mu\text{m}$  and larger represents a diverse set of biological (e.g., viruses, bacteria, and protozoa) and nonbiological materials (e.g., clays, oxides, etc.).

**Mechanisms of Excess Deposition Efficiency.** Previously, it was hypothesized that the excess  $\alpha$  in porous media was

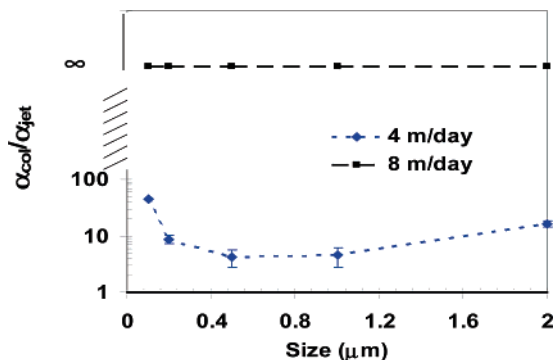


**FIGURE 5.** Ratio of deposition efficiency in the porous media versus the impinging jet system as a function of particle size and fluid velocity at an ionic strength = 0.02 M and pH = 6.72 (ionic strength = 0.05 M for the 2.0  $\mu\text{m}$  microspheres). Error bars represent standard deviations in results from replicate experiments ( $n = 2$ ).

attributable to the presence of rear flow stagnation zones (12–17). Straining and wedging are other potential deposition mechanisms that may be associated with pore throats grain-to-grain contacts, respectively (8–10, 19, 20, 35). However, the colloid/collector diameter ratios examined here (0.0002–0.0039) are well below traditionally suggested ratios that would lead to straining, e.g., 0.05 (33, 34), and are also below the recently suggested threshold ratio of 0.005 for straining based on experiments (8) and for wedging based on experiments and simulations (19, 20, 35), suggesting that mechanisms other than wedging and straining contribute to excess  $\alpha$  in this system.

**Trends in Excess Deposition Efficiency.** Based on the expectation of increased fluid drag with increasing fluid velocity, one would expect that the largest ratios of  $\alpha$  (column/jet) would correspond to the highest fluid velocities. This expectation was confirmed (Figure 5), where the ratios increased to infinity as the fluid velocity was increased to 8  $\text{m day}^{-1}$ .

Based on the expectation of increased fluid drag with increasing colloid size, one would expect that the largest ratios of column/jet  $\alpha$  would correspond to the largest colloids. However, the results (Figure 5) demonstrated that this ratio was actually largest for the smallest colloids (0.1  $\mu\text{m}$ ). This observation indicates that the probability of retention in flow stagnation zones is greater for smaller microspheres, e.g., they experience lesser fluid drag, and occupy less space per colloid, relative to larger microspheres. Rear flow stagnation points have previously been considered too limited to retain significant numbers of colloids (1). However, recent mechanistic particle tracking simulations incorporating fluid drag, diffusion, and colloidal forces simulated the retention of microspheres (less than about 1.5  $\mu\text{m}$  in radius) in flow stagnation zones in spherical porous media (35), providing a mechanistic basis for the phenomenon, and prompting further investigation via incorporation of colloid–colloid interactions.

**Effect of Collector Angularity.** Deposition in the absence of an energy barrier is approximately a factor of 2 higher in quartz sand relative to equivalently sized glass beads (Table 1, 19–22), reflecting the greater surface area present on angular relative to spherical collectors. However, this effect of collector angularity on deposition is minor relative to that observed in the presence of an energy barrier, which yields order of magnitude differences in deposition between angular versus spherical collectors (19–22). In agreement with these studies, a factor of 5 greater  $\alpha$  was observed in quartz sand relative to glass beads (both 510  $\mu\text{m}$  diameter collectors) for the 0.5  $\mu\text{m}$  diameter microspheres ( $\sim 0.001$  colloid/collector ratio) (4  $\text{m day}^{-1}$  fluid velocity) (Table 1).

**Reversibility of Excess Deposition.** Release of retained microspheres upon introduction of low ionic strength solution (0.0002 M) was significant in the porous media (15–40%) but was negligible in the impinging jet (Table 1, and Supporting Information). This observation demonstrates that a portion of the excess retention of colloids in the porous media was reversible with respect to decreased solution ionic strength, indicating that the colloids were associated with grain surfaces via the secondary energy minimum in the porous media (12–17). Colloid release (re-entrainment) in the absence of ionic strength or other perturbations was also significant in the porous media, but was insignificant in the impinging jet (Table 1, and Supporting Information), further suggesting that a significant fraction of the excess retained colloids were not in direct physical contact with collector surfaces, and further implicating zones of flow stagnation as important locations of colloid retention in porous media.

**Implications.** Our results demonstrate that excess deposition in porous media is relevant to a wide range of colloid sizes (0.1  $\mu\text{m}$  and larger) and occurs in porous media composed of spherical as well as angular grains. The magnitude of excess deposition increased with increasing fluid velocity, as expected. However, excess deposition was greatest for the smallest colloids (0.1  $\mu\text{m}$ ), possibly suggesting an increasingly limited capacity of the flow stagnation zones for larger colloids. The excess deposition observed in the porous media was a factor of 5–50 times greater than the deposition observed on equivalent flat surfaces, indicating that surface charge heterogeneity and roughness (a mechanism of barrier reduction or elimination ostensibly common to both systems) played minor roles relative to other potential retention mechanisms associated with pore domain geometry. A significant portion of the excess deposition was reversible with respect to ionic strength, indicating that retention involved reversible association with surfaces via the secondary energy minimum. Our results indicate that in the presence of an energy barrier (typical of environmental conditions) collector geometry is critical to deposition of a wide range of colloid sizes.

## Acknowledgments

This material is based upon work supported by the National Science Foundation Hydrologic Sciences Program (EAR 0337258). Any opinions, findings, and conclusions or recommendations expressed in this material are those of the author(s) and do not necessarily reflect the views of the National Science Foundation. We acknowledge three anonymous reviewers for their very positive and helpful comments.

## Supporting Information Available

Details about porous media and column preparation, impinging jet preparation, fluid velocity scaling between column and impinging jet systems, representative deposition flux curve from impinging jet experiments, DLVO characterization of colloid–collector interaction, verification of lack of aggregation via flow cytometry, and discussion of trends of colloid re-entrainment rate coefficients in porous media. This material is available free of charge via the Internet at <http://pubs.acs.org>.

## Literature Cited

- (1) Elimelech, M.; O'Melia, C. R. Kinetics of deposition of colloidal particles in porous media. *Environ. Sci. Technol.* **1990**, *24* (10), 1528–1536.
- (2) Song, L.; Elimelech, M. Dynamics of colloid deposition in porous media: modeling the role of retained particles. *Coll. Surf., A* **1993**, *73*, 49–63.
- (3) Song, L.; Elimelech, M. Transient deposition of colloidal particles in heterogeneous porous media. *J. Colloid Interface Sci.* **1994**, *167*, 301–313.

- (4) Johnson, P. R.; Sun, N.; Elimelech, M. Colloid transport in geochemically heterogeneous porous media: Modeling and measurements. *Environ. Sci. Technol.* **1996**, *30* (11), 3284–3293.
- (5) Bhattacharjee, S.; Ko, C. H.; Elimelech, M. DLVO interaction between rough surfaces. *Langmuir* **1998**, *14*, 3365–3375.
- (6) Shellenberger, K.; Logan, B. E. Effect of molecular scale roughness of glass beads on colloidal and bacterial deposition. *Environ. Sci. Technol.* **2002**, *36* (2), 184–189.
- (7) Bradford, S. A.; Simunek, J.; Bettahar, M.; Tadassa, Y. F.; van Genuchten, M. T.; Yates, S. R. Straining of colloids at textural interfaces. *Water Resour. Res.* **2005**, *41*, doi:10.1029/2004WR003675.
- (8) Bradford, S. A.; Bettahar, M.; Simunek, J.; van Genuchten, M. Th. Straining and attachment of colloids in physically heterogeneous porous media. *Vadose Zone J.* **2004**, *3*, 384–394.
- (9) Bradford, S. A.; Yates, S. R.; Bettahar, M.; Simunek, J. Physical factors affecting the transport and fate of colloids in saturated porous media. *Water Resour. Res.* **2002**, *38* (12), 1327–1338.
- (10) Bradford, S. A.; Simunek, J.; Bettahar, M.; van Genuchten, M. T.; Yates, S. R. Modeling colloid attachment, straining, and exclusion in saturated porous media. *Environ. Sci. Technol.* **2003**, *37*, 2242–2250.
- (11) Tufenkji, N.; Ryan, J. N.; Harvey, R. W.; Elimelech, M. Transport of *Cryptosporidium* Oocysts in porous media: role of straining and physicochemical filtration. *Environ. Sci. Technol.* **2004**, *38*, 5932–5938.
- (12) Franchi, A.; O'Melia, C. R. Effects of natural organic matter and solution chemistry on the deposition and reentrainment of Colloids in Porous Media. *Environ. Sci. Technol.* **2003**, *37*, 1122–1129.
- (13) Hahn, M. W.; Abadzic, D.; O'Melia, C. R. Aquasols: On the role of secondary minima. *Environ. Sci. Technol.* **2004**, *38*, 5915–5924.
- (14) Hahn, M. W.; O'Melia, C. R. Deposition and reentrainment of Brownian particles in porous media under unfavorable chemical conditions: some concepts and applications. *Environ. Sci. Technol.* **2004**, *38*, 210–220.
- (15) Walker, S. L.; Redman, J. A.; Elimelech, M. Role of cell surface Lipopolysaccharides (LPS) in *Escherichia coli* K12 adhesion and transport. *Langmuir* **2004**, *20*, 7736–7746.
- (16) Redman, J. A.; Walker, S. L.; Elimelech, M. Bacterial adhesion and transport in porous media: role of the secondary energy minimum. *Environ. Sci. Technol.* **2004**, *38*, 1777–1785.
- (17) Brow, C.; Li, X.; Ricka, J.; Johnson, W. P. Comparison of microsphere deposition in porous media versus simple shear systems. *Colloids Surf., A* **2005**, *253*, 125–136.
- (18) Johnson, W. P.; Tong, M. Observed and simulated fluid drag effects on colloid deposition in the presence of an energy barrier in an impinging jet system. *Environ. Sci. Technol.* **2006**, *40* (16), 5015–5021.
- (19) Li, X.; Lin, C. L.; Miller, J.; Johnson, W. P. Pore-scale observation of microsphere deposition at grain-to-grain contacts over assemblage-scale porous media domains using X-ray microtomography. *Environ. Sci. Technol.* **2006**, *40* (12), 3762–3768.
- (20) Li, X.; Lin, C. L.; Miller, J.; Johnson, W. P. Role of grain-to-grain contacts on profiles of retained colloids in porous media in the presence of an energy barrier to deposition. *Environ. Sci. Technol.* **2006**, *40* (12), 3769–3774.
- (21) Li, X.; Scheibe, T. D.; Johnson, W. P. Apparent decreases in colloid deposition rate coefficient with distance of transport under unfavorable deposition conditions: a general phenomenon. *Environ. Sci. Technol.* **2004**, *38* (21), 5616–5625.
- (22) Li, X.; Johnson, W. P. Nonmonotonic variations in deposition rate coefficients of microspheres in porous media under unfavorable deposition conditions. *Environ. Sci. Technol.* **2005**, *39* (6), 1658–1665.
- (23) Tong, M.; Camesano, T. A.; Johnson, W. P. Spatial variation in deposition rate coefficients under unfavorable deposition conditions resulting from non-electrostatic mechanisms. *Environ. Sci. Technol.* **2005**, *39* (10), 3679–3687.
- (24) Tong, M.; Li, X.; Brow, C.; Johnson, W. P. Detachment-influenced transport of an adhesion-deficient bacterial strain within water-reactive porous media. *Environ. Sci. Technol.* **2005**, *39* (8), 2500–2508.
- (25) Zhang, P.; Johnson, W. P.; Scheibe, T. D.; Choi, K.; Dobbs, F. C.; Mailloux, B. J. Extended tailing of bacteria following breakthrough at the Narrow Channel Focus Area, Oyster, Virginia. *Water Resour. Res.* **2001**, *37* (11), 2687–2698.
- (26) Scheibe, T. D.; Wood, B. D. A particle-based model of size or anion exclusion with application to microbial transport in porous media. *Water Resour. Res.* **2003**, *39* (4), doi:10.1029/2001WR001223.
- (27) Rajagopalan, R.; Tien, C. Trajectory analysis of deep-bed filtration with the sphere-in-cell porous media model. *AIChE J* **1976**, *22* (3), 523–533.
- (28) Rajagopalan, R.; Tien, C.; Pfeffer, R.; Tardos, G. Letter to the editor. *AIChE J* **1982**, *28*, 871–872.
- (29) Tufenkji, N.; Elimelech, M. Correlation equation for predicting single-collector efficiency in physicochemical filtration in saturated porous media. *Environ. Sci. Technol.* **2004**, *38*, 529–536.
- (30) Kern, W.; Poutinen, D. Cleaning solutions based on hydrogen peroxide for use in silicon semiconductor technology. *RCA Rev.* **1970**, *31*, 187–206.
- (31) Li, X.; Zhang, P.; Lin, C. L.; Johnson, W. P. Role of hydrodynamic drag on microsphere deposition and re-entrainment in porous media under unfavorable conditions. *Environ. Sci. Technol.* **2005**, *39* (11), 4012–4020.
- (32) Johnson, W. P.; Li, X.; Assemi, S. Hydrodynamic drag influences deposition and re-entrainment dynamics of microbes and non-biological colloids during non-perturbed transport in porous media in the presence of an energy barrier to deposition. *Adv. Water Resour.* **2006**, Special Issue, doi:10.1016/j.advwatres.2006.05.020.
- (33) Sakthivadivel, R. *Theory and Mechanism of Filtration of Non-Colloidal Fines Through a Porous Medium*; Hydraulic Engineering Laboratory, University of California: Berkeley, CA, 1966.
- (34) Sakthivadivel, R. *Clogging of a Granular Porous Medium by Sediment*; Hydraulic Engineering Laboratory, University of California: Berkeley, CA, 1969.
- (35) Johnson, W. P.; Li, X.; Yal, G. Colloid retention in porous media: mechanistic simulations of wedging and retention in zones of flow stagnation. *Environ. Sci. Technol.*, in review.

Received for review May 18, 2006. Revised manuscript received September 17, 2006. Accepted September 20, 2006.

ES061201R